Solid-State ^{1}H NMR Relaxation Analysis of Ultrahigh Molecular Weight Polyethylene Reactor Powder

Hiroki Uehara,* Taku Aoike, Takeshi Yamanobe, and Tadashi Komoto

Department of Chemistry, Gunma University, Kiryu, Gunma 376-8515, Japan

Received March 15, 2001; Revised Manuscript Received October 4, 2001

ABSTRACT: Solid-echo ^{1}H NMR relaxation was analyzed for ultrahigh molecular weight polyethylene reactor powders. Their high crystallinities reveal the characteristics of crystalline free induction decay (FID). We propose here a very simple but appropriate fitting function for the crystalline component: combination of Weibullian and sine functions. The applicability of this function was tested for the series of samples having much higher crystallinity of over 90%, which was achieved by fuming nitric acid etching at room temperature over a period of 1 year. The typical beat at 20−30 μs on the observed FID was further emphasized by prolongation of etching time, which corresponds to "crystalline" relaxation. An introduction of the simple Weibullian/sine function for FID fitting reproduces well this beat profile. On the other hand, the FID relaxation of the amorphous chains could be represented by the single Weibullian function. However, they were classified into two categories: intermediate and mobile, depending on their relaxation characteristics. Among these three components (crystalline, intermediate, and mobile ones) exhibiting different chain motions, the intermediate amorphous relaxation was an effective guide for characterization of phase arrangements in our powder samples. The component percentage of this phase decreased with prolongation of the etching time, which was coincident with the crystallinity development detected by thermal analysis. Also, the spin−spin relaxation time of intermediate amorphous chains gradually decreased with the progress of the etching treatment. These results indicate that the molecular motion of the surviving intermediate amorphous phase is restricted. A comparison of morphological changes and these FID characteristic transformations obtained during etching suggested that such an intermediate amorphous phase is located in the region between crystalline domains within the powder globules.

Introduction

For semicrystalline polymers, it is widely accepted that several phases, including crystalline and amorphous phases, coexist within a sample. One of the major differences among these phases lies in their molecular dynamics. Several methods, such as thermal analysis and X-ray measurement, can quantitatively characterize these different phases; however, their analytical results are usually limited to information concerning the crystalline phase. In contrast, ^{1}H NMR relaxation analysis enables separate evaluation of crystalline and amorphous molecular dynamics. The individual scaling factors, including relaxation time scale, component percentage, and decay functions, can be compared among the phases contained in the sample, based on the ^{1}H NMR technique.

For decomposition of the observed ^{1}H NMR free induction decay (FID), the analytical formula of the crystalline decay has been often discussed because it exhibits a unique beat profile around 20−30 μs for polyethylene (PE).[1−9] Recently, Kristiansen et al.[5−7,9] characterized phase changes during melting and crystallization for high-density PE, linear low-density PE, and polypropylene by ^{1}H NMR FID analysis using the decay function calculated for the crystalline relaxation by Look et al.[10] Such a theoretical approach enables us to interpret the characteristics of crystalline relaxation. However, the analytical difficulties for this resolution technique lie in the complicated formula of the theoretical decay functions, containing multiple equations.

* To whom correspondence should be addressed. Telephone: +81-277-1332; Fax: +81-277-1333; e-mail: uehara@chem.gunma-u.ac.jp.

On the other hand, an application of the combination of Gaussian and sine functions for the crystalline decay[11] also brings a satisfactory fitting result in the case of ^{1}H NMR FID analysis of these crystalline polymers.[1,4,8,12,13] An introduction of this function was preferred for its simple formula, compared to that of the theoretical ones, which significantly reduces the calculation time for the profile fitting. In our previous study,[12] we also applied this simple Gaussian/sine function for ^{1}H NMR relaxation analysis of ultrahigh molecular weight (UHMW) PE samples. However, for the highly crystalline sample, for example, crystallized under high pressure into extended chain crystals, the simple Gaussian/sine function alone cannot represent the crystalline decay; thus, very "rigid" amorphous decay is additionally required for the profile fitting, but the spin−spin relaxation time (T_2) of such virtual amorphous decay sometimes is less than the crystalline one.[1]

One of the purposes of this work is to propose a more appropriate, but analytical, function for the crystalline relaxation, which can be easily applied for FID fitting, compared to the theoretical function. UHMW-PE reactor powder was selected because of its high crystallinity, which may emphasize the characteristics of crystalline decay. The series of further highly crystalline samples were prepared by fuming nitric etching. The fitting effectiveness was compared when different decay functions were introduced for FID resolution of these highly crystalline samples. Here, the higher surface area of reactor powder geometry is favored for acceleration of etching, compared to the flat surfaces of the bulk films or pellets.

The amorphous decay function has also been discussed because it is widely accepted that several amor-

10.1021/ma010464x CCC: $22.00
Published on Web 02/28/2002

phous phases, having different relaxation characteristics, coexist within semicrystalline polymers.[1−9,13−18] If such different amorphous phases allow corresponding acid diffusion, due to each molecular motion, the gradual etching may lead to the selective surviving of certain amorphous phases with higher resistance. This means that the comparison of FID analytical results between the series of the etched samples also predicts the appropriate decay function for each amorphous phase. For this purpose, a mild etching at room temperature (RT) was employed and examined over a period of 1 year to detect a gradual change of the sample FIDs. In contrast, rapid etchings at elevated temperatures have been examined in most of previous reports[1,14,17,19−23] because only the remaining crystals are focused.

Attention was also paid to the relaxation characteristics of unique structures contained in the reactor powder samples. It has been reported that crystallization during polymerization results in fibrils, whiskers, ribbons, and globules for semicrystalline polymers.[24−33] However, their individual properties have not been measured. On the basis of morphological changes during our fuming nitric acid etching treatment, the obtained solid-state NMR relaxation characteristics were assigned to some structural features of the UHMW-PE reactor powder.

Experimental Section

Materials. The samples tested were as-polymerized reactor powders of linear UHMW-PE Hifax 1900 from Montel with a weight average MW (M_w) of 2.6×10^6. The initial crystallinity estimated from density measurement was 81%, assuming a crystal/amorphous two-phase model.

Etching Treatment. Fuming nitric acid etching of reactor powders was performed at RT for up to 18 months. An excess amount of fuming nitric acid (10 mL) was added to 0.2 g of the powder sample in a glass bottle. As the etching proceeds, the strength of the acid is reduced by the reaction with PE. Thus, every month, the used acid was removed, and 10 mL of fresh acid was again added to the bottle. After treatment for a given period of time, the treated sample was washed with distilled water and then with acetone and dried well at RT.

Measurements. The molecular characteristics of the series of initial and etched powders were analyzed by gel permeation chromatography (GPC) in a solvent of 1,2,4-trichlorobenzene at Tosoh (Yokkaichi, Japan) using standard methods. MW characteristics, including M_w and number-average MW (M_n), were estimated from the measured GPC curves. MW distribution was evaluated as M_w/M_n.

The untreated and treated powders were characterized by DSC measurements. Thermograms were recorded from 80 to 180 °C at a heating rate of 3 °C/min. All scans were made under a N_2 gas flow using a Seiko DSC-10 DSC. The fraction crystallinities were calculated from the heat of fusion (ΔH_f). For this calculation, the enthalpy value of 290 J/g was used as that of perfect crystals of PE.[34] Both temperatures and endothermic areas were calibrated by indium and tin standards.

Scanning electron microscope (SEM) observations of untreated and treated samples were made using a Hitachi type S-5000 field-emission electron microscope operated at 5 kV. For transmission electron microscope (TEM) observations, a JEOL 1200EXS electron microscope was operated at 80 kV. The samples were stained by RuO_4 vapor and embedded in epoxy resin. The assembly was cut into thin sections 60 nm thick, using a Reichert UltraCut S. microtome.

^{1}H NMR measurements were carried out using a JEOL MU-25 solid-state pulse NMR spectrometer with a 25 MHz magnetic field. The FID was recorded by the solid-echo method. Data were collected every 0.2 μs. The dead time before signal sampling and interpulse spacing was 2 and 8 μs, respectively. The measured temperature was always RT. Obtained FID plots were analyzed by functional resolution into several components.

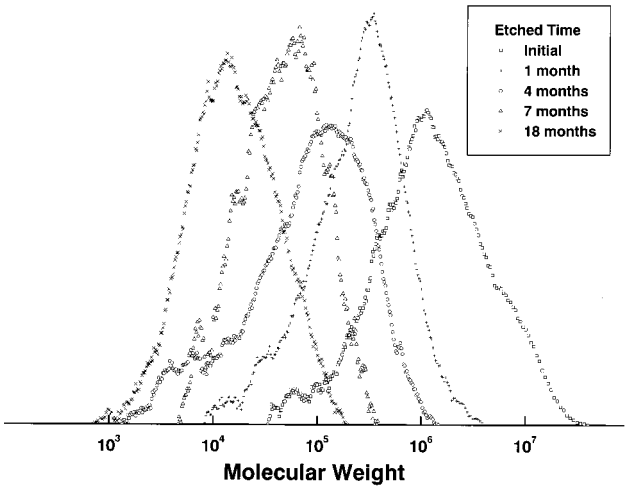

Figure 1. GPC chromatograms of the series of initial and etched UHMW-PE reactor powder samples. The etching times are indicated.

Results and Discussion

MW Characteristics of the Sample Powders. Usually, fuming nitric acid etching does not destroy the crystalline region. In such a case, an etching at elevated temperature is preferred for the rapid etching progress. The MW drops to the crystalline stem length within a shorter treatment time; thus, distribution curves duplicate each other even if different treatment times were examined.[23,35] In contrast, the gradual elimination of the amorphous chains is required here in order to classify the multiple amorphous phases, with respect to their individual acid resistance. Thus, a lower-temperature treatment at RT was employed in this work. The RT etching requires a longer time to get a fully etched state,[33] but such a series of the etched samples can test various functions for FID fitting, as discussed later.

The progress of etching at RT for the UHMW-PE reactor powder used was followed by GPC measurements. Figure 1 compares MW distribution curves for the series of initial and etched UHMW-PE reactor powder samples. All of these chromatograms exhibit a similar single peak. However, this peak gradually shifts to lower MW with increasing etching time. The initial powder has a peak maximum in the UHMW region over 10^6. The low MW tail of this chromatogram is negligible below 10^4. In contrast, for the powder etched over 7 months, the high MW tail never exceeds 10^6. These features mean that the etching proceeds homogeneously within the sample powder morphology, independent of treatment time.

The M_w, M_n, and MW distribution (M_w/M_n) calculated from these GPC profiles are summarized in Table 1. The initial M_w of 2.6×10^6 and M_n of 5.6×10^5 gradually decrease with increasing etching period, reaching 2.4×10^4 and 1.0×10^4 for the 18-month-etched powder. A crystalline stem length of ~ 30 nm for the initial powder, which is evaluated from TEM observation later, corresponds to a MW of $\sim 3 \times 10^3$. Full removal of the amorphous phase should give this minimum MW after

Table 1. Molecular Weight Characteristics of the Series of Initial and Etched UHMW-PE Reactor Powders

sample	$10^{-4}M_n$	$10^{-4}M_w$	M_w/M_n
initial	56	260	4.7
1 month etched	13	38	3.0
4 month etched	2.8	16	5.5
7 month etched	3.1	6.4	2.1
18 month etched	1.0	2.4	2.5

etching. Namely, even for the powder etched for prolonged period, certain amorphous components still survived under the mild treatment examined in this work.

Morphological Changes during Etching. Powder morphologies of both the initial and etched samples were also characterized. SEM and TEM observations are effective to detect the morphological changes in the powder surface and internal structures, respectively, during etching. Figure 2 shows sets of low- and high-magnification SEM images for the initial and 4- and 12-month-etched UHMW-PE powders. Unique "cobweb" structures, composed of globules and fibrils, are often observed on the surfaces of as-polymerized PE reactor powders;[23,26,32,33] however, very few fibrils are recognizable for the powder examined here, as shown in the high-magnification image of Figure 2d. Instead, the pastelike structures cover the surface of this reactor powder. The major powder morphology consists of globules with radii of a few micrometers, independent of etching time. After etching for more than 4 months, the pastelike structure on the powder surface almost disappeared (see Figure 2e), and grain structures are slightly recognizable within each globule. Further treatment for 12 months enables clear separation of such grains with radii of ~30 nm, as shown in Figure 2f. This means that the regions located between these grains were gradually sculpted with increasing the etching time.

Figure 3 shows sets of low- and high-magnification TEM images for the initial and 4- and 12-month-etched UHMW-PE powders. For TEM observation, the amorphous chains were stained by RuO_4; thus, the bright regions correspond to the crystalline components. From the high-magnification image of the initial powder (Figure 3d), it is found that these crystalline components exhibit distributed domain morphologies rather than the usual lamellar structure observed for the solution- or melt-crystallized PE.[12] These crystalline domains have a size of ~30 nm, which corresponds well to the radii of grains recognized in SEM images of the 18-month-etched powder (see Figure 2f). Increasing etching time leads to the lower phase contrast in the TEM images (Figure 3e,f) because the amorphous regions, which are stained dark, were gradually removed even from the interior of the powder during etching. The simultaneity of the surface and internal morphological changes suggest that a mild etching proceeds homogeneously within the whole of the powder, regardless of the geometrical position within a powder.

FID Resolution Analysis. Quantitative phase analyses of the series of UHMW-PE powders were also made from ^{1}H NMR FID profiles, assuming different decay functions. The fitting effectiveness of the introduced decay function was evaluated by the deviation between the simulated and observed data plots. Figure 4 shows the ^{1}H NMR FIDs for the series of initial and etched UHMW-PE powders. Here, the normalized magnetization intensity is plotted using a logarithmic

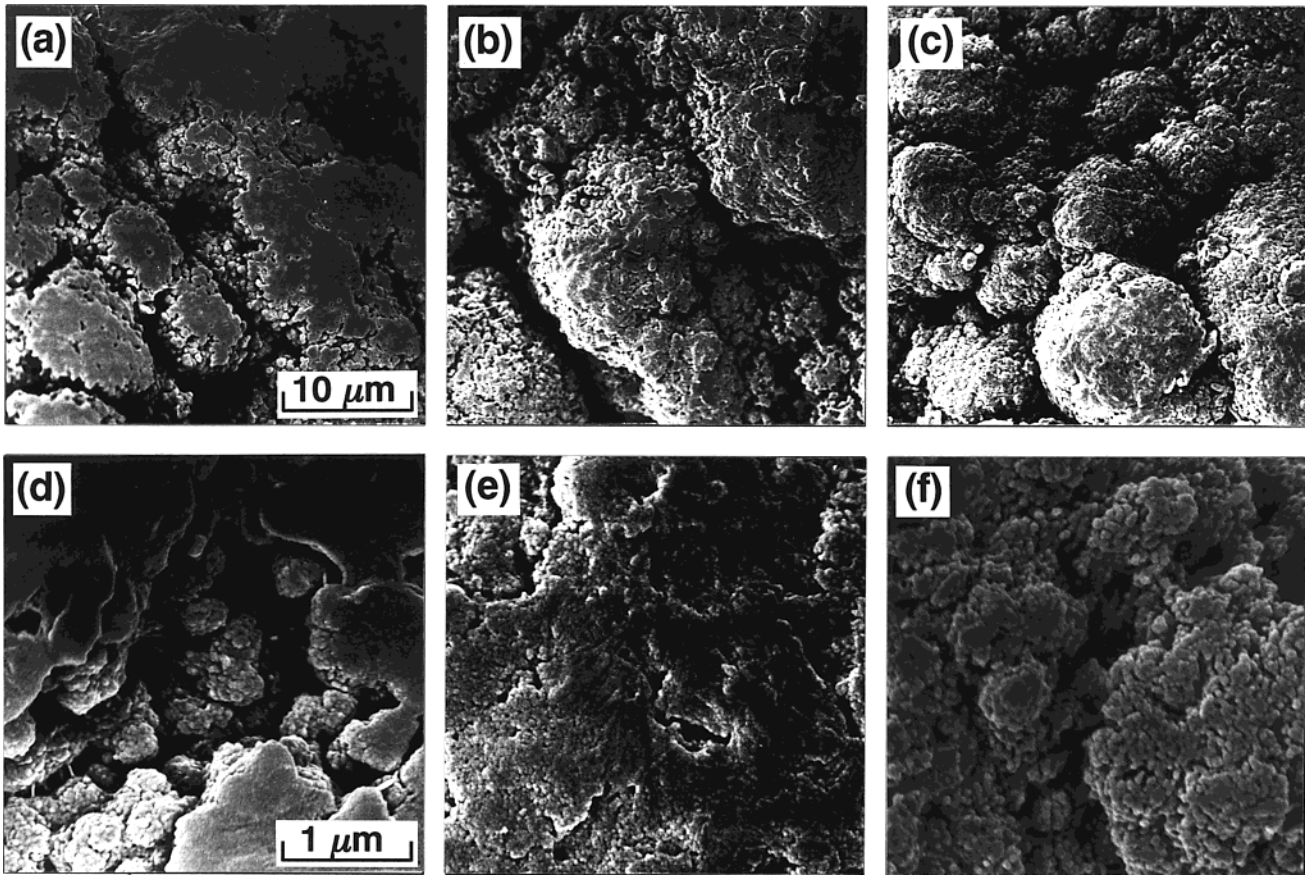

Figure 2. Scanning electron microscopic images of the series of UHMW-PE samples: initial powder (a, d), powder treated for 4 months (b, e), and powder treated for 12 months (c, f). Top and bottom views are low- and high-magnification images, respectively.

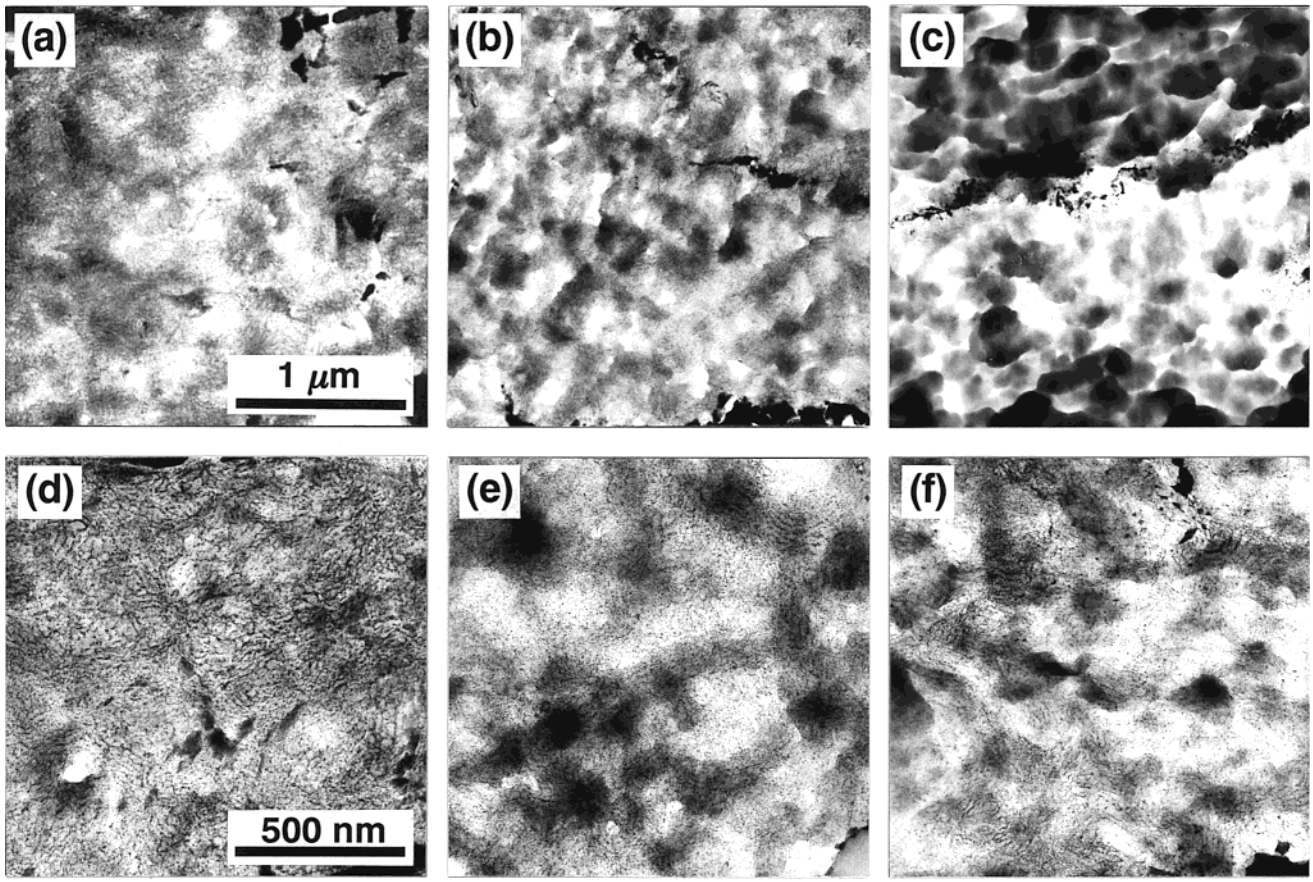

Figure 3. Transmission electron microscopic images of the series of UHMW-PE samples: initial powder (a, d), powder treated for 4 months (b, e) and powder treated for 12 months (c, f). Top and bottom views are low- and high-magnification images, respectively.

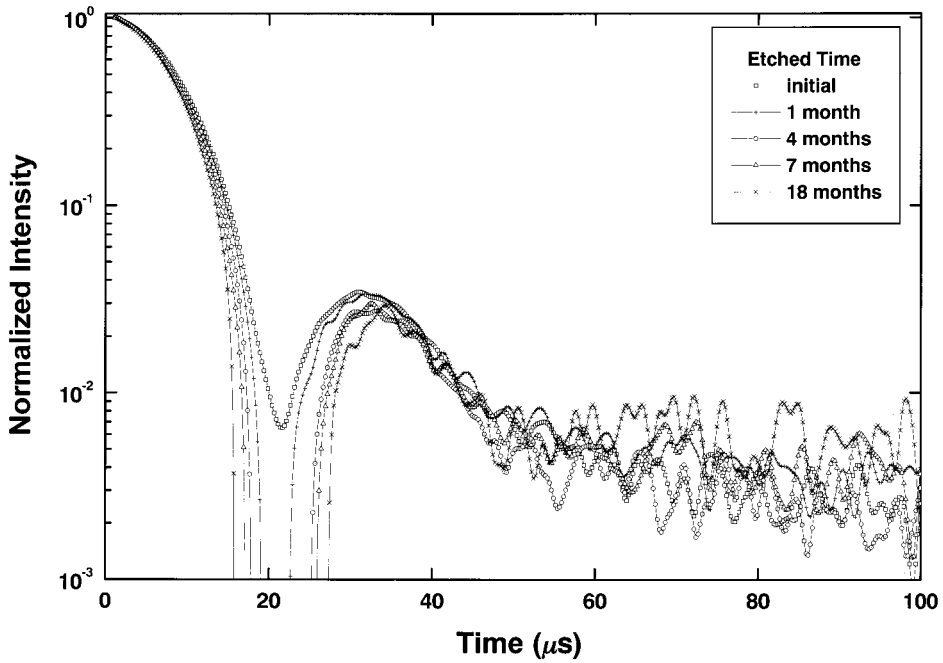

Figure 4. Comparison of FIDs observed at RT for initial UHMW-PE powder and series of samples etched for various periods of time from 1 to 18 months.

scale to emphasize the characteristic "beat" around 20 μs. This beating profile becomes more prominent with increasing etching time. As shown later, the sample crystallinity also increases with increasing treatment time. Thus, it is reasonable to attribute this beating to one of the crystalline decay characteristics.

Similar beating profiles are often observed for inorganic crystals. In such a case, the position of the beat minimum is ascribable to the dipole−dipole pair distance in the crystals. This assignment of beat position is given by theoretical interpretation of Fourier transformed broad-line profile shape[10] on a frequency scale,

the so-called Pake doublet.[36] The doublet peak tops separate with a certain interval reflecting the dipole−dipole pair distance in the crystals. This doublet spectrum is broadened by the distribution of remaining, weaker dipole interactions in the crystals. Abragam[11] showed that such a crystalline FID is represented by the combination of Gaussian and sine functions, as follows:

$$I_1(t) = A_1 \exp\left\{-\frac{(k_1 t)^2}{2}\right\}\frac{\sin bt}{bt} \qquad (1)$$

where t is the decay time and I is the normalized magnetization intensity. The Gaussian part in this function arises from the distribution of dipole interactions. This Gaussian/sine equation is an appropriate fitting function for the crystalline component of solution- or melt-crystallized UHMW-PE samples.[8,12]

To test the fitting effectiveness of which this function represents the crystalline decay, the most crystalline sample was selected, namely, the 18-month-etched powder having the highest crystallinity in this study. In FID deconvolution even for such highly crystalline samples, the amorphous component will still be required for better profile fitting. This is expected from GPC results, which indicate that full etching of the amorphous phases has not been completed even after an 18-month-etching period (see Figure 1). For the amorphous FID, the exponential decay function is widely used to express molecular relaxation. RT is well above the glass transition temperature of PE; thus, the rapid rotation of the amorphous chains averages out the dipolar interactions in the amorphous phases. This effect leads to the Lorentzian-type exponential decay function for the amorphous relaxation. However, Lorentzian decay sometimes deviates from the observed amorphous FID plots. Weibullian exponential decay, containing the power coefficient d_2, can represent the various types of amorphous relaxation curves from Lorentzian ($d_2 = 1$) to Gaussian ($d_2 = 2$) decays, as follows.[37]

$$I_2(t) = A_2 \exp\left\{-\frac{(k_2 t)^{d_2}}{2}\right\} \qquad (2)$$

Figure 5a shows the FID resolutions into crystalline and amorphous decays, assuming the combination of decay functions of eqs 1 and 2. The resolved decays for crystalline and amorphous components are also shown. A slight deviation between the fitted and observed plots was recognizable, especially for the signal around 40 μs. Such a deviation can be clearly revealed in the residual signal plots shown in the inset of Figure 5a. Some beating still remains, above the noise, on the residual signal plots. Further, the assignments of the crystalline and amorphous decays involve a contradiction in this case. The crystalline relaxation defined by eq 1 should be much more rigid than the amorphous one by eq 2; however, the amorphous T_2 calculated from the FID resolution in Figure 5a was 15.3 μs, which is comparable to 14.3 μs of the crystalline T_2. (The details of the T_2 calculation will be described in the next section.)

In contrast, the simulated curve in Figure 5b is in good agreement with the observed FID. In this fitting, the crystalline decay function was modified, considering the actual deviation of the dipole interaction from Gaussian distribution. The introduction of Gaussian function in eq 1 is based on the prediction by Pake[36] for

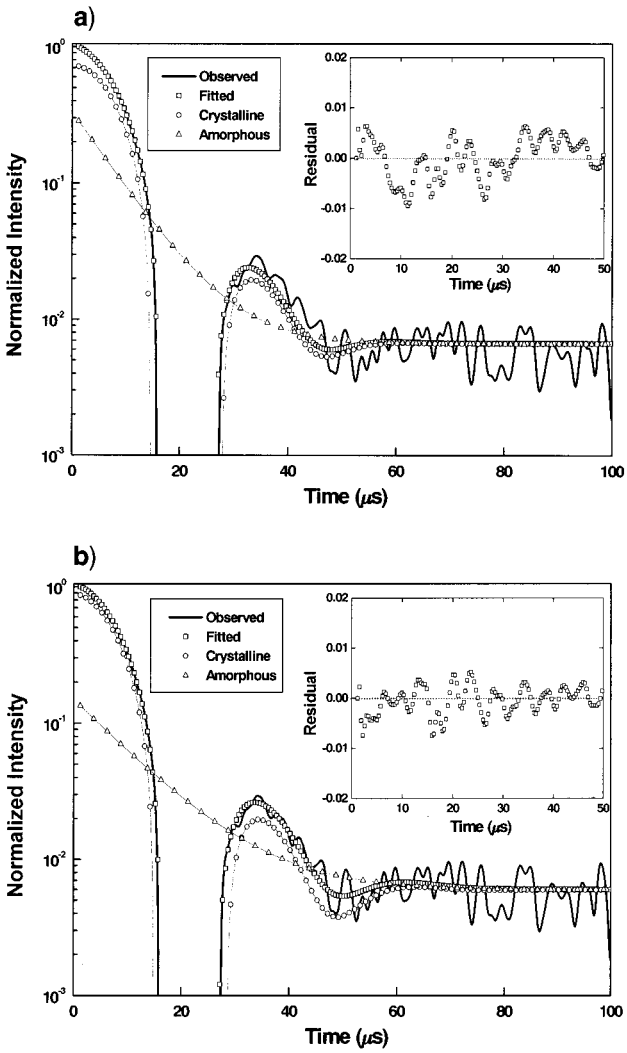

Figure 5. FID resolutions into crystalline and amorphous decays for the powder etched for 18 months, assuming different sets of the decay functions: (a) Gaussian/sine for crystalline and Weibullian for amorphous relaxations, given by eqs 1 and 2, respectively; (b) Weibullian/sine for crystalline and Weibullian for amorphous relaxations, given by eqs 3 and 2, respectively. The inset figures show the residuals between observed and fitted plots at the beat region (0−50 μs).

crystals of small molecules, such as 1,2-dichloroethane, where dipole pairs are isolated each other. However, in the polymeric materials, not only the dipole interactions between the nearest neighbors but also those between the proton pairs with longer distance contribute to the FID profile shape. Therefore, the distribution of the dipole interaction may be distorted. Thus, we constrained the ideal Gaussian distribution into Weibullian form, as follows:

$$I_3(t) = A_3 \exp\left\{-\frac{(k_3 t)^{d_3}}{2}\right\}\frac{\sin bt}{bt} \qquad (3)$$

where d_3 is the power coefficient introduced for the Weibullian part. Here, d_3 of 2 can give the conventional Gaussian/sine function. Figure 5b shows the results of the profile fitted by using eq 3 for the crystalline decay and eq 2 for the amorphous phase in the case of the powder etched for 18 months. The resolved profiles for crystalline and amorphous components are also shown. The agreement between the fitted and observed plots

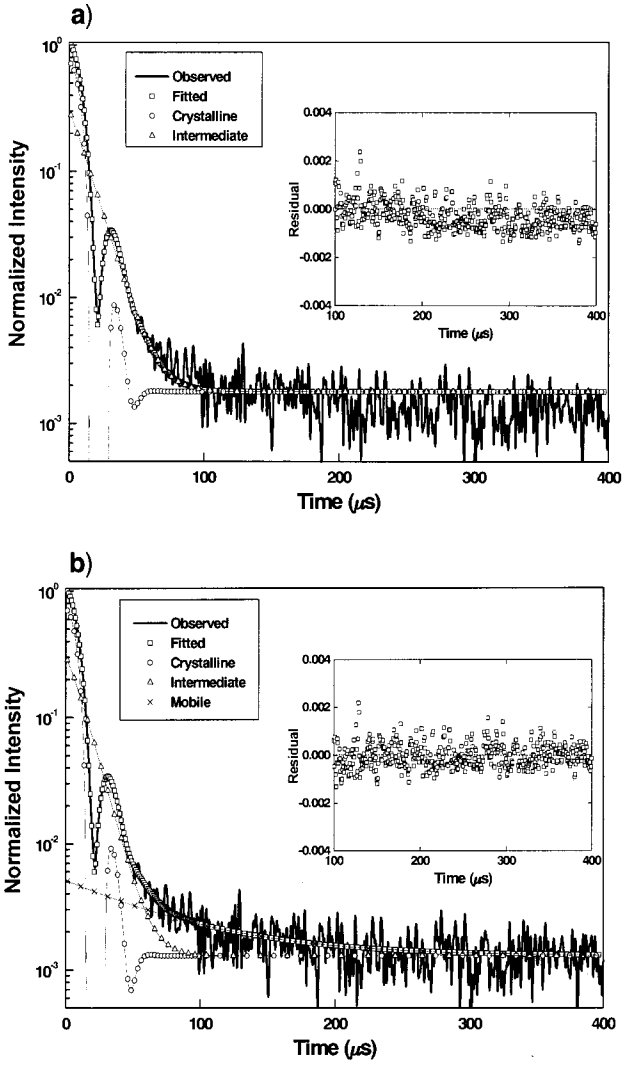

Figure 6. FID resolutions into two and three components for the initial unetched powder: (a) crystalline and intermediate components; (b) plus additional mobile component. Fitting functions for crystalline component and for intermediate or mobile component are given by eqs 3 and 2, respectively. The inset figures show the residuals between observed and fitted plots at the long decay region (100−400 μs).

is much improved, compared to Figure 5a. This can be clearly recognized from the residual signal data shown in the inset of the figure.

For FID resolution of the initial powder, such two-phase fitting (crystalline + amorphous) resulted in a slight difference from the observed data plots, especially on a longer time scale (over 100 μs), as shown in Figure 6a. The residual signal plots shown in the inset figure still have a slope remaining in the longer time range of 100−400 μs. Thus, additional amorphous relaxation was introduced for the initial powder. Corresponding to the decay time categories of these two amorphous phases, the former and the latter were defined as "intermediate" and "mobile" components, respectively, in this work. A combination of Weibullian/sine (crystalline component: eq 3) and two Weibullian decays (intermediate and mobile amorphous components: eq 2) was applied for fitting. Figure 6b shows the results of profile fitting, assuming these three-component functions for the initial powder. The residual signal plots shown in inset of the figure exhibit zero slope, except for the spectrum noise. The intensity of the additional "mobile" amorphous

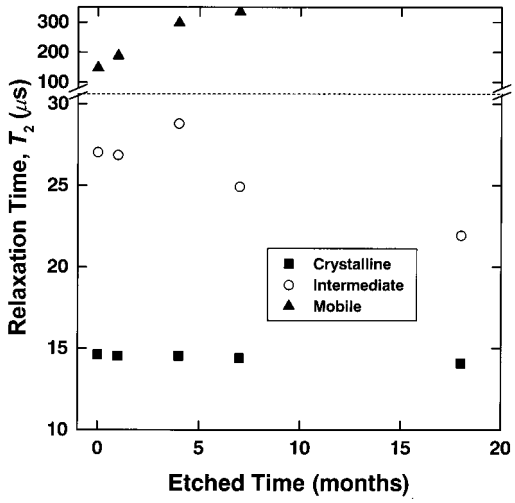

Figure 7. Etching time dependencies of T_2 for the series of initial and etched powders. Both values for crystalline and two amorphous (intermediate and mobile) relaxations were plotted for each sample.

decay was very small, less than 1%, which can be estimated from the intercept across the ordinate axis, but it should again be noted that the addition of this function seemed to be required for better fitting in the longer time region over 100 μs in the case of the untreated reactor powder. A similar three-component detection has been reported for solid-state ^{13}C NMR measurements of UHMW-PE samples.[38−41]

There is an advantage in using this Weibullian/sine decay function for the analytical ease of FID resolution. The $b = 0$ in this function leads to simple Weibullian decay. Then, the Gaussian and Lorentzian decays, which are usually assumed as the amorphous relaxation functions, can be also represented when $d_2 = 2$ and 1, respectively. In other words, the Weibullian/sine function covers all types of the decay functions assumed here, regardless of the phase characteristics.

^{1}H NMR Relaxation Characteristics Changes. Similar FID analyses were applied to the other etched powders. From these profile fittings, spin−spin relaxation times (T_2) were estimated. For simple Lorentzian or Gaussian decay, we defined T_2 to be the reciprocal of the integral peak width (the length of the horizontal line which equally divides the total area of the peak) in a Fourier transformed broad-line spectrum. The corresponding analysis was also carried out for crystalline Weibullian/sine or intermediate Weibullian decay. When the Weibullian power coefficient, d_2 or d_3, was 1 or 2, the Weibullian/sine or simple Weibuillian function can be Fourier transformed in closed form. However, except for such cases, the scattered points simulated by each resolved function were numerically Fourier transformed on a frequency scale. The integral peak widths were estimated from these simulated broad-line spectra, and then T_2's were calculated.

The T_2 obtained for each decay function is plotted in Figure 7 as a function of etching time. For a highly crystalline powder etched for 18 months, only a single amorphous decay represented by the Weibullian function was required for the desirable fitting, as shown in Figure 5. The T_2 of this component lies around ~22 μs, which implies very limited molecular motion, compared to that of usual amorphous PE chains (~200 μs). Thus, this relaxation component was attributed to the "intermediate" amorphous chains. In contrast, a satisfactory

FID fitting for the initial powder having lower crystallinity requires the additional "mobile" amorphous component, as shown in Figure 6. In other words, longer etching completely removes this mobile amorphous component. Concurrently, one observes a disappearance of the pastelike morphology on the powder surface (see Figure 2). The T_2 of the mobile amorphous component changes between 100 and 300 μs, which is comparable to the values for amorphous relaxation times in the case of conventional melt-crystallized UHMW-PE.[12] This phase was below 1%, as evidenced by its low intensity in Figure 6b. Thus, the quantitative interpretation of T_2 for this component is difficult. However, it should be noted that such a small amount of this phase is coincident with the fact that the pastelike morphologies, as seen in SEM images for the initial powder, seem to spread on the powder surface, rather than in the globular interior (compare Figures 2 and 3) and almost disappeared in the earlier stage of etching.

In Figure 7, it can be also seen that the crystalline T_2 has a constant value around 14.5 μs, independent of etching time. The reason for the constant crystalline T_2 is that the mobility of the crystalline component is not affected by the etching or that the correlation time for the crystalline component is in the extremely slow region where T_2 is insensitive to the chain mobility. In both cases, the mobility of the crystalline component is slow enough to maintain the crystalline structure. This means that the crystalline region remains undamaged during mild etching. In contrast, the intermediate amorphous T_2 shows a rapid decrease with prolongation of etching time. Prolonged etching for 18 months finally gives the shortest intermediate amorphous T_2 near 22 μs among those estimated in this work. This phase simultaneously decreased from 17% for the initial powder to 7% for the 18-month-etched sample, which was estimated from the areas in the Fourier transformed broad-line spectra. These unique characteristics of the intermediate amorphous region with prolongation of etching time can be reasonably compared to the results obtained from SEM and TEM observations. With increasing etching time, the regions located between the crystalline grains were gradually removed, as shown in Figures 2 and 3. This means that such regions correspond to the intermediate amorphous components. The decreasing T_2 value for this component suggests that the molecular motion of the surviving intermediate amorphous phase is restricted. Among the intermediate amorphous chains, the region far from the crystalline domains can be destroyed earlier, but more restricted chains that are connected with crystalline domains just at phase boundaries may survive even after prolonged etching.

Crystallinity Changes during Etching. Figure 8 compares the crystallinity changes estimated from ^{1}H NMR analysis and DSC measurements for a series of the etched powders. The crystallinity values for ^{1}H NMR analysis were calculated from the areas in the Fourier transformed broad-line spectra, simulated for the crystalline, intermediate amorphous, and mobile amorphous relaxation decays. Those for DSC measurements were calculated from the heat of fusion. Both estimation methods show parallel increases in the crystallinity with increasing etching time. The crystallinity changes estimated from ^{1}H NMR FID analysis was a gradual increase from initial ~83% to final ~93%. This 10% increase in crystallinity also agrees well with that estimated from DSC. Such coincidence between ^{1}H NMR and DSC data confirms that the decay functions employed here for FID resolution are desirable for the phase analysis of the UHMW-PE reactor powder samples in this study.

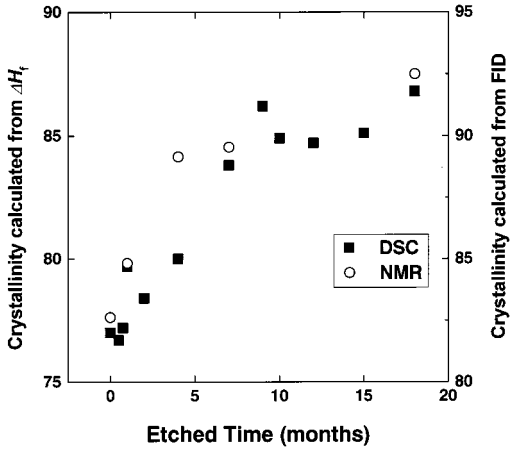

Figure 8. Comparison of etching time dependencies of crystallinity, estimated from DSC and ^{1}H NMR FID analyses for the series of initial and etched powders. For the latter case, the percentage of the crystalline component is plotted.

Conclusions

A series of highly crystalline samples was prepared by a mild fuming nitric acid etching of the UHMW-PE reactor powder. A gradual progress of the chain scission was confirmed by GPC data for the series of etched samples. Several decay functions were tested for profile resolution of the emphasized crystalline FID. Among these functions, a combination of Weibullian and sine functions could be applied to represent the characteristic crystalline relaxation profile having significant beat composition. The molecular motion in the crystalline region as reflected in the corresponding T_2 values remained constant for the entire treatment period. A simultaneous increase in crystallinity could be inferred by such ^{1}H NMR analysis, consistent with DSC results. It was also found that the initial reactor powder sample contains two amorphous components having quite different T_2's: mobile and intermediate. Both of these amorphous decays could be reproduced by the Weibullian function. A combination of morphological observation by electron microscopy and relaxation analysis by ^{1}H NMR FID indicates that the mobile amorphous component is attributed to the pastelike phase, which covers the surface of the initial powder. This mobile amorphous component completely disappears during mild etching. In contrast, the intermediate amorphous decay still remains even after prolonged etching. The gradual removal of the region located between crystalline domains during the later treatment period corresponds to the decrease of component percentage and T_2 value for this intermediate amorphous decay. Such a unique phase arrangement and restricted molecular motion of the amorphous chains are characteristic of reactor powder structure and properties.

Acknowledgment. This work was partly supported by Industrial Technology Research Grant Program in '00 from the New Energy and Industrial Technology Development Organization (NEDO) of Japan.

References and Notes

(1) Klüver, W.; Ruland, W. *Prog. Colloid Polym. Sci.* **1978**, *64*, 255.
(2) Voigt, G.; Kimmich, R. *Polymer* **1980**, *21*, 1001.
(3) Kamel, I.; Charlesby, A. *J. Polym. Sci., Polym. Phys. Ed.* **1981**, *19*, 803.
(4) Bergman, K.; Schmiedberger, H.; Unterforsthuber, K. *Colloid Polym. Sci.* **1984**, *262*, 283.
(5) Hansen, E. W.; Kristiansen, P. E.; Pedersen, B. *J. Phys. Chem. B* **1998**, *102*, 5444.
(6) Kristiansen, P. E.; Hansen, E. W.; Pedersen, B. *J. Phys. Chem. B* **1999**, *103*, 3552.
(7) Kristiansen, P. E.; Hansen, E. W.; Perdersen, B. *Polymer* **2000**, *41*, 311.
(8) de Langen, M.; Luigjes, H.; Prons, K. O. *Polymer* **2000**, *41*, 1183.
(9) Kristiansen, P. E.; Hansen, E. W.; Pedersen, B. *Polymer* **2001**, *42*, 1969.
(10) Look, D. C.; Lowe, I. J.; Northby, J. A. *J. Chem. Phys.* **1966**, *44*, 2441.
(11) Abragam, A. *Principles of Nuclear Magnetism*; Clarendon: Oxford, 1961.
(12) (a) Uehara, H.; Yamanobe, T.; Komoto, T. *Macromolecules* **2000**, *33*, 4861. (b) Uehara, H.; Matsuda, H.; Aoike, T.; Yamanobe, T.; Komoto, T. *Polymer* **2002**, *42*, 5393.
(13) Dadayli, D.; Harris, R. K.; Kenwright, A. M.; Say, B. J.; Sünnetcioğlu, M. M. *Polymer* **1994**, *35*, 4083.
(14) Bergman, K.; Nawotki, K. *Kolloid Z. Z. Polym.* **1966**, *219*, 132.
(15) Loboda-Čačković, V. J.; Hosemann, R.; Wilke, W. *Kolloid Z. Z. Polym.* **1969**, *235*, 1263.
(16) Phaovibul, O.; Loboda-Čačković, J.; Čačković, H.; Hosemann, R. *Makromol. Chem.* **1974**, *175*, 2991.
(17) Kitamaru, R.; Horii, F.; Hyon, S.-H. *J. Polym. Sci., Polym. Phys. Ed.* **1977**, *15*, 821.
(18) Bergmann, K. *J. Polym. Sci., Polym. Phys. Ed.* **1978**, *16*, 1611.
(19) Olf, H. G.; Peterlin, A. *Kolloid Z. Z. Polym.* **1967**, *215*, 97.
(20) Cryst, B.; Peterlin, A. *J. Polym. Sci., Part A-2* **1969**, *7*, 1165.
(21) Bergmann, K. *Polym. Bull. (Berlin)* **1981**, *5*, 355.
(22) Phillips, R. A. *J. Polym. Sci., Polym. Phys. Ed.* **1998**, *36*, 495.
(23) Cook, J. T. E.; Klein, P. G.; Ward, I. M.; Brain, A. A.; Farrar, D. F.; Rose, J. *Polymer* **2000**, *41*, 8615.
(24) Blais, P.; Manley, R. St. J. *J. Polym. Sci., Part A-1* **1968**, *6*, 291.
(25) Keller, A.; Willmouth, F. M. *Makromol. Chem.* **1969**, *121*, 42.
(26) Graff, R. J. L.; Kortleve, G.; Vonk, C. G. *J. Polym. Sci., Polym. Lett.* **1970**, *8*, 735.
(27) Chanzy, H. D.; Revol, J. F.; Marchessault, R. H.; Lamandé, A. *Kolloid Z. Z. Polym.* **1973**, *251*, 563.
(28) Moñoz-Escalona, A.; Parada, A. *J. Cryst. Growth* **1980**, *48*, 250.
(29) Smith, P.; Chanzy, H. D.; Rotzinger, B. P. *J. Mater. Sci.* **1987**, *22*, 523.
(30) Kakugo, M.; Sadatoshi, H.; Sakai, J.; Yokoyama, M. *Macromolecules* **1989**, *22*, 3127.
(31) Tervoort-Engelen, Y. M. T.; Lemstra, P. J. *Polym. Commun.* **1991**, *32*, 343.
(32) Nooijen, G. A. H. *Eur. Polym. J.* **1994**, *30*, 11.
(33) Uehara, H.; Nakae, M.; Kanamoto, T.; Ohtsu, O.; Sano, A.; Matsuura, K. *Polymer* **1998**, *39*, 6127.
(34) Wunderlich, B.; Cormier, C. M. *J. Polym. Sci., Part A-2* **1967**, *5*, 987.
(35) Weeks, N. E.; Mori, S.; Porter, R. S. *J. Polym. Sci., Polym. Phys. Ed.* **1975**, *13*, 2031.
(36) Pake, G. E. *J. Chem. Phys.* **1948**, *16*, 327.
(37) Brereton, M. G. *J. Chem. Phys.* **1991**, *94*, 2136.
(38) Chen, W.; Fu, Y.; Wunderlich, B.; Cheng, J. *J. Polym. Sci., Polym. Phys. Ed.* **1994**, *32*, 2661.
(39) Cheng, J.; Fone, M.; Reddy, V. N.; Schwartz, K. B.; Fisher, H. P.; Wunderlich, B. *J. Polym. Sci., Polym. Phys. Ed.* **1994**, *32*, 2683.
(40) Fu, Y.; Chen, W.; Pyde, M.; Londono, D.; Annis, B.; Boller, A.; Habenschuss, A.; Cheng, J.; Wunderlich, B. *J. Macromol. Sci., Phys.* **1996**, *B35*, 37.
(41) Kuwabara, K.; Kaji, H.; Horii, F.; Bassett, D. C.; Olley, R. H. *Macromolecules* **1997**, *30*, 7516.

MA010464X